CEAS Aeronautical Journal
https://doi.org/10.1007/s13272-026-00959-x

ORIGINAL PAPER

# Atmospheric testing of hydrogen fuel injectors for RQL combustion within the Rolls-Royce Pearl 15 hydrogen demonstrator engine program

Johannes Berger[1] · Thomas Behrendt[1] · Sebastián Eisenring[1] · Bertram Janus[1] · Carsten Clemen[2]

Received: 28 May 2025 / Revised: 9 January 2026 / Accepted: 2 March 2026


**Abstract**
Five swirl stabilized hydrogen injectors for aviation propulsion rich-quench-lean combustion were provided by Rolls-Royce Deutschland to the DLR Institute of Propulsion Technology. The injectors are tested at atmospheric pressure and combustor-like test conditions. Cameras in the infrared and ultraviolet wavelengths are applied to record water-vapor and OH* radiation respectively. The images are averaged, deconvoluted and overlaid. All injectors are found to stabilize at lean and rich test conditions. Flame stabilization was observed in the shear layer of the inner recirculation zone and, in some cases, in the shear layer of the outer recirculation. In variant 1 and 2, the fuel is introduced within two air flows and interacts with both. Fast mixing of air and fuel was the design objective. Variant 3–5 are designed to achieve locally fuel rich and thus colder regions. Variant 3 is designed for centrally injected low velocity fuel and produces a V-shaped flame. Variant 4 and 5 also feature a central fuel injection, but with a radial velocity component. Fuel and air mix more intense than in V3 and distinct combustion brushes form. Variant 2 and 5 are shown with a shortened seal which eliminates flame anchoring on the seal, but also removed the flow widening effect. Based on the experimental results, it is concluded that hydrogen flames stabilize well in a kerosene-derived swirl injector with high blow-off resilience. The objective of good mixing for variant 1 and 2 was achieved, likewise locally fuel rich regions created for variant 3–5.

**Keywords** Jet engine · Hydrogen combustion · Hydrogen burner · Rich quench lean (RQL) · Swirl stabilized · Rich combustion

## 1 Introduction

Man-made global warming is shown in many aspects of our current climate, such as extreme weather phenomena [1]. Hydrogen can potentially decarbonize aviation and thus reduce direct carbon dioxide emissions of aircraft. Challenges arise not only from the low volumetric energy density and thus storage space on board [2], but also from the altered combustion behaviour compared to well analysed carbon-based fuel burning systems [3]. The application of understood so-called Rich-Quench-Lean (RQL) combustion systems for a safety-oriented application in jet engines is reasonable given the challenges of hydrogen's altered combustion characteristics. Especially rich diffusion flames, as they are applied in aviation RQL combustors, burning pure hydrogen are not yet studied in detail. Applied liquid jet fuel injectors are fine-tuned systems with great effort put into spray performance. Examples can be found

✉ Johannes Berger
johannes.berger@dlr.de

Thomas Behrendt
thomas.behrendt@dlr.de

Sebastián Eisenring
sebastian.eisenring@dlr.de

Bertram Janus
bertram.janus@dlr.de

Carsten Clemen
dr.carsten.clemen@rolls-royce.com

[1] The Institute of Propulsion Technology, German Aerospace Center (DLR), Linder Höhe, 51147 Cologne, North Rhine-Westphalia, Germany

[2] Rolls-Royce Deutschland Ltd. & Co. KG, Eschenweg 11, 15827 Blankenfelde-Mahlow, Brandenburg, Germany

Published online: 16 March 2026

in [4–7]. The introduction of high-volume flow hydrogen to jet engine injectors requires significant changes as visible within the multitude of designs presented in this study, and thus makes a direct comparison in between hydrogen and kerosene injectors impractical. Studies on hydrogen jet engine fuel injectors with drop-in capabilities beside the presented are not publicly available, but research on academic burners is being conducted. The so-called HYLON burner combines swirl stabilization with non-premixed injection of hydrogen and air, as shown for instance in [8] and [9]. A succeeding injector with three flow paths can be found in [10]. A swirl number study, albeit on premixed combustion, is available in [11]. Flashback and Blow-Off is ivestigated in [12] and the effect of pressure on hydrogen combustion described in [13]. An interesting setup with two air flow paths is numerically studied in [14]. Contrary to the presented injectors, none of the quoted hydrogen burners is as application-oriented.

Flame stability seems to be less difficult to achieve as hydrogen shows much wider flammability limits [15]. But this can lead to the flame anchoring close to the injector outlet and potentially high thermal loads. Another unknown is the thermoacoustic response of the hydrogen flame, which has shown to be altered for increased hydrogen content, for example in [16].

For this purpose, hydrogen injectors for aviation gas turbines are tested and data about their combustion performance is acquired. Each injector is tested under atmospheric pressure throughout a variation of power settings and two series of line-of-sight images in the infrared and ultraviolet spectrum capturing water vapor and OH* radicals are recorded. These low technology readiness level (TRL) tests show the potential and challenges of hydrogen and give early insight into the performance, the design implications, and the sensitivities of different non-premixed swirl stabilized injector designs. The goal of this test campaign is to establish a low-TRL-filter to identify the most promising hydrogen injectors to proceed with in the high-pressure test campaign.

The lower pressure and lower temperature need to be considered when assessing the findings of the study for engine application. An increase in both will increase the thermal load of the combustion chamber. The position of the reaction zone is influenced by a higher engine like preheat temperature. The general flame shape is expected to be constant as described in [13], but a more realistic liner contour and mixing module as in [17] will affect the flow field. An increase in emissions of nitrogen oxides, as described by [13], is likely. The later experiments at higher TRL in sector [17] and full annular rigs [18] confirmed the general findings presented in this paper.

The used injectors are developed by RRD and described in [17–19] as well as the following section. All injectors are meant for state-of-the-art RQL combustion chambers of the mid-sized Pearl 15 engine [19]. The presented paper is describing the initial atmospheric testing to establish a low-TRL-filter in the Atmospheric Primary Zone (APZ) test bed analysing only the near injector area within the rich primary zone for all five injectors at ambient pressure.

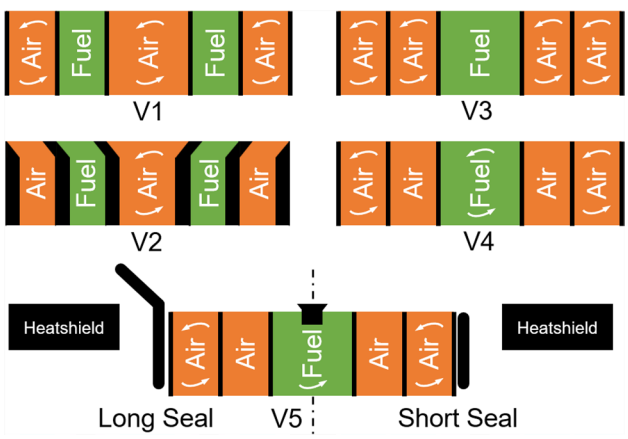


**Fig. 1** Air and fuel flow paths in all injector variants with swirl indicators and schematic half cuts of short and long seal

## 2 Hydrogen injectors

Using CFD-Tools yielded a total of five designs with similar overall CFD-predicted $NO_x$ emissions developed by RRD. The so-called variant 1 to variant 5 (V1–V5) injectors were all newly developed, but orient themselves on their kerosene equivalents (compare to [5]). Due to these similarities, the results are valid for typical gas turbine combustor fuel injector diameters in the range of 25–50 mm. The underlying design objective was to prevent the flame from anchoring on the injector by reaching a certain hydrogen outlet velocity and to gain a broad understanding of swirl-stabilized hydrogen combustion.

The most prominent difference between the injectors is the position of the hydrogen outlet, as schematically shown in Fig. 1. Variant 1 and 2 feature a slit in between an inner and outer air stream to inject hydrogen . This setup is chosen to ensure fast and good mixing. Variant 3–5 have a central fuel supply for simplified manufacturing. Due to the large central outlet, V3 fails to achieve high outlet velocities for hydrogen. It was developed to understand the limitations for rich combustion and flame stabilization in hydrogen diffusion flames. V4 and V5 were designed to achieve locally fuel rich regions and limiting $NO_x$ emissions by reducing the temperature in these regions. Compared to kerosene, where soot production in very rich regions limits the design space, hydrogen offers, through its absence of carbon and

wide combustibility limits, the chance to reduce the flame temperature by further reducing the local air-fuel-ratio (AFR). All five injectors are shown in Fig. 2 and all swirlers are co-rotating. The simulations found in Fig. 3 of [19] imply that V1 and V2 have a temperature field similar to kerosene injectors where hotter gas fills out the primary zone much more compared to V3, V4, and V5, where the reaction in the primary zone seems colder and the temperature unevenly distributed. This agrees with the described design objectives of V1 and V2 achieving fast mixing contrary to V4 and V5, which aim at achieving locally fuel rich regions. Additionally, the simulation revealed that the flame might interact with the kerosene seal, called *Long Seal* in Fig. 1, thus another shortened seal, marked *Short Seal*, was manufactured.

### 2.1 Injectors V1 and V2: fast mixing

V1 features an inner and outer air swirler with swirl-free hydrogen injection in between both air streams by means of a continuous slit. Both air flows rotate in the same direction. Current kerosene injectors of RRD feature three concentric air swirlers. In a descriptive approximation one could say that the hydrogen outlet, which increased in size compared to kerosene due to the low density of hydrogen, replaced the middle swirler. Similarly, V2 features two air flows with a continuous slit of hydrogen in between. The hydrogen passage features no swirl as in V1, but contrary to V1, the outer air passage imprints no swirl on the airflow and is considerably smaller. The inner air passage of V2 features a cone shaped segment which presumably functions as a diffusor for the inner air stream. The fuel and outer air outlet are angled outwards leading to a radial velocity component despite no swirler being present. The underlying assumption was that less swirl could improve thermoacoustic performance and thus other design features were implemented to achieve a wide flame, enabling a short primary zone and stability through recirculation, without swirl.

### 2.2 Injectors V3–V5: locally fuel rich

The injectors V3–V5 are designed to inject fuel centrally surrounded by two air streams. The simplest fuel inlet can be found in V3, which is a relatively large central tube and two co-rotating swirling air flows around. This injector fails to meet the criterion of a high hydrogen outlet velocity and showed instabilities regarding the location of the flame region in the simulations. Nevertheless, this injector showed no $NO_x$ penalty in the simulation. The injector V4 changed compared to V3 in regards to a swirler within the now smaller central fuel passage as well as having only one air swirler which is in the outer air stream. The objective of a high exit velocity of hydrogen is met. The air passage without swirl in between inner fuel passage and outer swirled air is implemented to prevent flame anchoring on the hydrogen outlet. Notably, the separation in between fuel and inner air path is equipped with a sharp edge. The only alternation from V4 to V5 is the elongation of the hydrogen swirler hub to function as a bluff body ending with a small deflecting lip. Simulations showed a region of low velocity in the injector central axis of V4 due to the imposed swirl, which is suppressed by the bluff body of V5 [18, 19].


**Fig. 2** Tested hydrogen injectors V1–V5 [19]

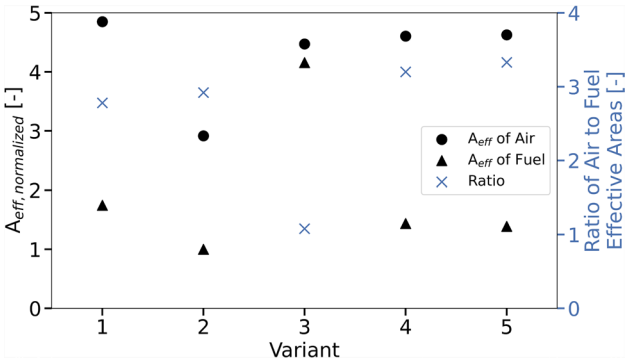


**Fig. 3** Normalized air and fuel effective area and ratio

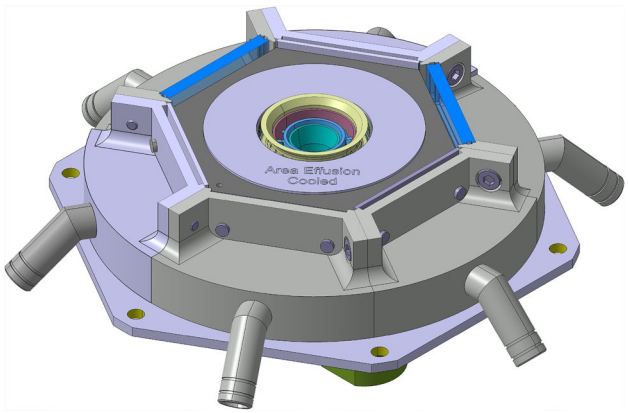


**Fig. 4** Low cut through the combustion chamber walls. V1 and the long seal are mounted in the heat shield with covered effusion cooling holes

### 2.3 Effective area

All injectors are tested for their effective area on a separate test bed prior to the combustion tests. The injectors are fitted into an enclosed space providing a uniform, slow inlet flow, discharging into the atmosphere and respectively the air or fuel flow path is blocked off. The effective area is measured using compressed air for multiple pressure drops and averaged. The formula used is

$$A_{eff} = \frac{\dot{m}}{\sqrt{2\Delta p \rho}} \tag{1}$$

with the massflow $\dot{m}$, the pressure drop $\Delta p$ and the density $\rho$. The shown incompressible results agree with the compressible formulation. It needs to be noted that the effective areas are all measured with no flow through the fuel path when measuring the air path and vice versa.

The stark difference in some geometric features of the injectors is mirrored in their effective areas, as can be seen for both the air and fuel outlets in Fig. 3. The effective area of the air flow path is within a ten percent deviation for V1, V3, V4 and V5. As expected from the geometry assessment, it is almost identical for V4 and V5. Outstanding is the air passage effective area for V2. Since the injectors are all tested at the same pressure drop and at the same AFR, the smaller effective area of V2 leads to a lower air and fuel mass flow. As expected, outstanding regarding the fuel flow is V3. The fuel outlet is almost as large as the air outlet, which means that the fuel velocity is significantly lower than that of the other injectors at the same conditions. The injectors V1, V4 and V5 are again within a similar absolute range of fuel passage effective area, but taking the ratio in between air and fuel path effective areas (marked × in Fig. 3) into account shows that also V2 is within this group. Specifically, this ratio in between air and fuel flow paths increases through V1, V2, V4 and V5 by 17 %. This ratio is correlating to a decrease in momentum flux ratio and leads to a higher relative velocity in between the air and fuel flows and thus potentially different mixing behaviour. The bluff body of V5 seems to reduce the effective area of the fuel flow by about 3.5 %, although the geometric area blocked by the bluff body downstream of the swirler present in V4 and V5 is greater than 3.5 %.

## 3 Test environment

The tests are conducted using the infrastructure at the DLR test site in Cologne. The following subsections cover the test rig in Sect. 3.1, the camera setup in Sect. 3.2, and the test conditions in Sect. 3.3.

### 3.1 Test rig

The atmospheric pressure tests are conducted using the APZ test rig of the Institute of Propulsion Technology [20, 21] at the DLR in Cologne. The injector mounted in the heat shield with low cut walls is shown in Fig. 4. The combustion chamber ready for testing can be seen in Fig. 6 of [18].

The air and fuel flow paths in Fig. 5 are showing the preheated air entering the combustion chamber from the bottom in orange, the cold air in blue and hydrogen in green. The exhaust gas, in red, is depicted in the converging outlet of the combustion chamber which prevents backflow. The majority of the preheated air flows through the injector. Partly it is used as cooling for the heat shield and the injector seal. For confidentiality, the heat shield is covered in Fig. 4, but it employs a multitude of small and complexly shaped flow paths discharging on the heat shield surface. The seal with cooling holes can be seen in [5]. The injector AFR, and for this the fraction of preheated air passing through the injector, is calculated using the effective area previously measured for each injector and normalized by the maximum of the shown test points. The cold cooling

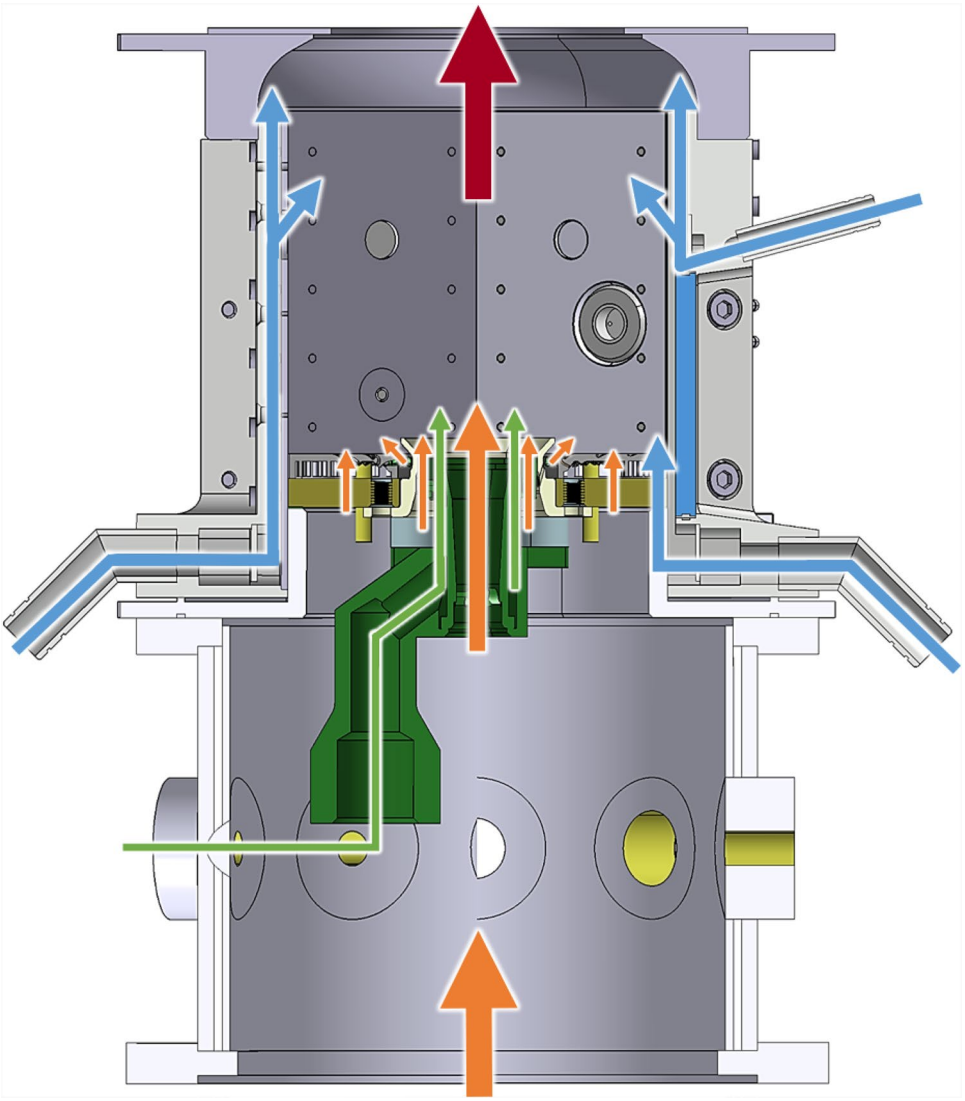

**Fig. 5** Vertical cross section of the APZ rig with flow paths of pre-heated air (orange), cold air (blue), hydrogen (green), and exhaust gas (red)

air (in blue) is supplied at ambient temperature and set to a fixed total mass flow for all conditions. Of the six wall elements forming the combustion chamber, two are equipped with windows. The airflow through these is introduced in two positions of the combustor: One functioning as cooling air film on the inner side of the window, and a second supply is partly injected into the combustion chamber as mixing air as well as used as convective cooling for the upper part of the wall downstream of the window and is injected close to the combustion chamber exit. This can be seen on the right side of Fig. 5. The other four wall elements, shown on the left side of Fig. 5, are all convectively cooled despite their different functionality.

The injector is mounted from the back, within the seal and centrally in the heat shield, and supplied with hydrogen at ambient temperature. At multiple locations both temperature and pressure are measured, such as the pressure within the plenum and the temperature of the heat shield.

### 3.2 Camera setup and image post processing

The hexagonal cross-sectioned combustion chamber including the camera angles is seen in Fig. 6. Recordings are taken with an ultraviolet (UV) camera (PCO Dicam Pro, 1280x1024 pixel with 2x2 binning, 100 mm UV lens, f/2.8) recording OH* chemiluminescence in between 305 and 325 nm. The camera is angled inwards to record the burner central axis despite the blockage of the window frame. The OH*-signal as marker for the heat release rate is described in [22–24] and applied at the DLR in [25].

Another camera (Xenics Xeva vSWIR, 320 × 256 pixel InGaAs detector with spectral range 500–1700 nm, OPTEC OB-V-SWIR 100 mm lens, f/2, 25 % transmissivity filter) is recording the infrared spectrum from 1330 to 1520 nm. The camera field of view is through both windows to exclude any background radiation of hot combustor parts. This means, as shown in Fig. 6, that the burner central axis is

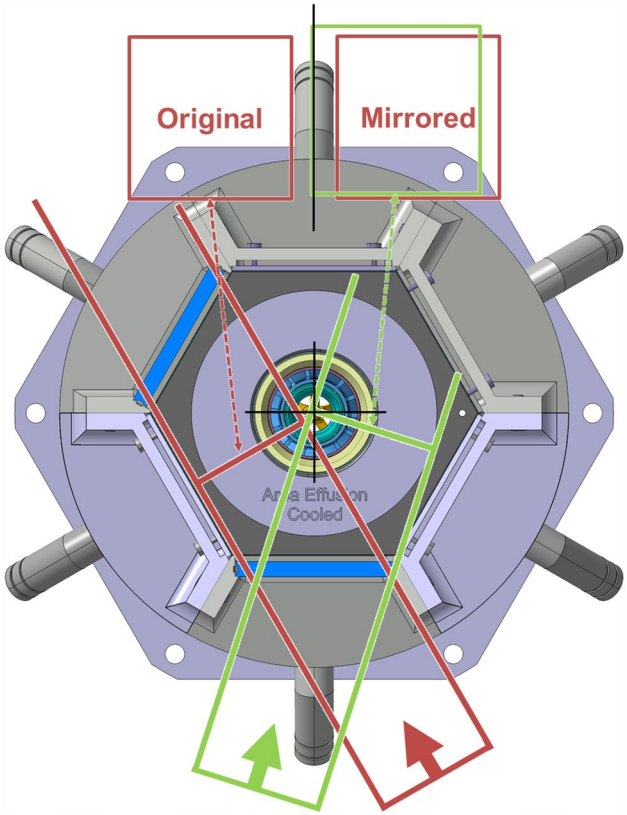


**Fig. 6** Vertical cross section of the APZ rig indicating the infrared, shown in red, and ultraviolet, in green, camera angles

not visible contrary to the UV camera image. Overlapping both cameras pictures thus shows the window frame and no signal on the central axis in the infrared spectrum. The angle of view effect causes the reflection on the inner surface of the seal to be visible, such as in Fig. 9b . The signal of water vapor within this band scales linearly with the volumetric concentration and non-linearly with the temperature, with a higher impact through temperature. The emissivity can be confirmed using the database in [26]. Regardless, water vapor as a combustion product will always be found at elevated temperature.

Both cameras record a sample of 400 line-of-sight images. Within post processing, the camera images are cropped, median filtered (3 × 3 for the UV-images and 5×5 for the IR-images), normalized by the exposure time and averaged into one single mean image. Additionally, the infrared image is mirrored. Both images are individually deconvoluted using the PyAbel package and the basex method [27]. Both images are then overlapped with the OH*-signal being displayed in the blue colour scheme and the $H_2O$ radiation as black contour lines.

**Table 1** Selected test conditions

| Sequence | dp [%] | $AFR_{injector}/AFR_{ref}$ [–] |
|---|---|---|
| Lean V1, V3–V5 | 4 | 2.56 (average) |
| Lean V2 | 4 | 1.8 |
| Rich V1–V5 | 4 | 1 |

### 3.3 Test points

Although the injectors show different key design features, all of them are tested following the same test routine reducing the air-fuel-ratio (AFR) from rich to lean and investigating lean extinction behaviour. The selected test points are shown in Table 1. Scaling of the fuel flows is based on the reduced mass flows, and the relative pressure drop is kept constant at a representative value for aircraft engine operation. An equivalent thermal load to kerosene is used to derive hydrogen AFRs and the test points cover a wide range of engine power settings from idle to take-off. As the experiments are conducted with gaseous fuel which inherently omits the evaporation phase, the lower preheat temperature has no strong influence on the stability analysis.

The injectors are ignited by a hydrogen torch at very lean conditions and a pressure drop of 4 %. The ignition process is smooth and the combustion is stable at very lean conditions for all tested variants. The leanest injector test point is measured at a normalized AFR of 2.61 with injector V5. Only the injector air is used to calculate the AFR within this paper.

The test bed infrastructure supplies preheated air up to 22.5 g/s at an average of 345 K. The air heater could not supply a consistent temperature due to a temporary malfunction. The highest preheat temperature is 373 K, the minimum is 324 K and the standard deviation through all test points is 10.5 K. The cold air mass flow on average is 25.5 g/s, with a maximum of 27.5 g/s, a minimum of 23 g/s and a standard deviation of 1 g/s. The maximum hydrogen mass flow of the infrastructure is 1.2 g/s continuously supplied, which was not reached in this campaign.

## 4 Flame stabilization

According to [28], a flame is stable if the range of input parameters, such as AFR, does not cause blow off or flashback. Within these limits, the flame stabilizes where the local flame propagation velocity and the flow velocity overlap.

### 4.1 Flow and flame velocity

Without further knowledge of the flow field, the only available velocity is the air and fuel outlet velocity of the injector. The air velocity is in between 60 and 90 m/s. The fuel

velocity through test conditions and effective areas spans from 20 to 250 m/s. The local velocity downstream of the outlet decreases due to the expansion of the flow, viscous effects and entrainment, which facilitate flame stabilization. The expansion at the injector outlet can cause a corner recirculation zone.

The flame propagation velocity correlates to the turbulent flame speed since the air flow Reynolds number of all test points is well within the turbulent regime. Within the described turbulent flows, a high rate of turbulent mixing occurs in regions of high velocity, pressure, and density gradients, such as the injector exit region. The mixing defines the local AFR and thus influences the flame velocity. Albeit not measured, a high degree of turbulent mixing is expected in the shear layer in between hydrogen and air streams of the presented injectors and in the shear layer between the fresh and recirculated gas. Theory on turbulent mixing can be, for example, found in [32] and [33]. Insights into mixing and turbulence in a representative liquid fuel jet engine injector can be found in [6]. As a reference, the experimentally found laminar flame speed of kerosene and hydrogen in regards to equivalence ratio are shown in Fig. 7. The kerosene reference is shown at 403 K [29] and the hydrogen reference is interpolated from [30, 31] at the lowest, highest, and mean preheat temperature. It can be seen that the laminar flame speed of hydrogen is significantly higher than the laminar flame speed of kerosene and also that the maximum is shifted towards richer conditions.

## 4.2 Rationale for the interpretation of the results

A set of principles for the interpretation of the presented pictures are stated in the following, as well as limitations described.

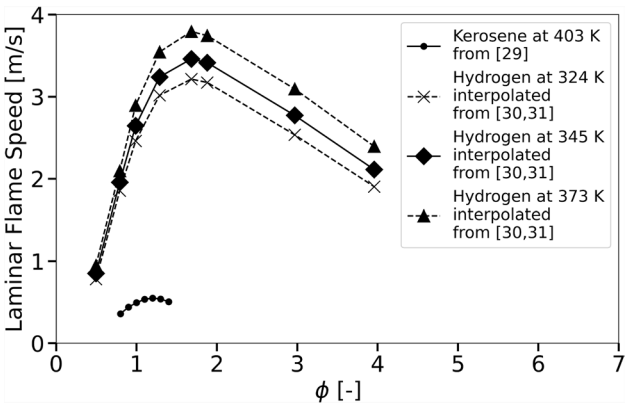


**Fig. 7** Comparison of laminar flame speed over equivalence ratio found in [29–31]

### 4.2.1 Ultraviolet signal showing the OH* radical

- The signal shows the average flame brush shape and position through the chemically excited OH* molecules as a marker for the reaction zone described by [22] and its position is linked to the fuel injection and flow field. This is for example applied to experimental data for swirl injectors by El Helou et al. [34] or Kruljevic et al. [35].
- The heat release can only occur at locations with adequate mixing due to the non-premixed introduction of fuel and air. Mixing is enhanced by turbulence and shear layers, and emissions increases, as shown by [22], when nearing stochiometry.
- The highest flame velocity benefiting flame stabilization found in the literature data lies at a rich AFR of 20.3 ($\Phi = 1.7$) as shown in Fig. 7.
- The volume flow increases with heat release.

### 4.2.2 Infrared signal of the water vapor radiation

- The signal shows hot and concentrated products of complete combustion, and the emissivity can increase respectively due to both, an increase in temperature or in concentration, as shown by [26].
- Hot combustion products are expected downstream of the flame region. A discussion comparing experimental results with CFD-results for a swirl injector can be found in [20].
- Temperature or concentration reduces due to mixing, shear, or other cooling effects such as a wall. The resulting stretching and wrinkling of the hot combustion gas contours are caused by the surrounding flow field or structure.

### 4.2.3 Conclusions based on the CFD simulation

The RANS simulations conducted for single test points can be used as an indicator for the flow field and combustion. The simulations were conducted using the Rolls-Royce proprietary code PRECISE-UNS as described in [19]. Based on the limited insight in the deployed code and the unavailability of all test points and hardware configurations, only the following guidelines can be defined:

- All injectors show a central recirculation zone of varying size and position, and the air flow dominates the combined flow field compared to the fuel flow.
- The CFD confirmed the expectation of potential flame anchoring at low velocity regions such as widening flow

fields and swirl induced shear layers transporting hot gas and radicals upstream.
- The highest heat release rate is found at fuel rich conditions, which correlates to the maximum flame velocity at an AFR of 20.3 ($\Phi = 1.7$) in Fig. 7.
- Employing the larger injector seal widens the flow field considerably and reduces the outer recirculation.

#### 4.2.4 Limitations

The interpretation of the images is limited through multiple factors, such as the mirroring and superposition of the images. This is possible due to the assumption that the flame is circumferentially symmetric, which is reasonable in the injector near field. Nevertheless, the influence of the cooling air film of the windows is different for both recorded images, which needs to be considered if analysing the near wall region. Also, the field of view itself with, in some cases, combustion and recirculation well beyond the visible area limits the possible interpretation. Generally, turbulent combustion is a highly instationary phenomena. Beér and Chigier [28] concluded that the spatial variation of both the flow velocity and the flame propagation velocity needs to be considered when discussing the flame stability. In agreement, [36] states that instantaneous position of the reaction zone can fluctuate greatly and thus the observed flame brush appears thicker on a time averaged image.

## 5 Test results

All injectors are stable at all test points. The weak extinction limit tests show extraordinarily lean flame out limits and, besides for V2, are defined by the lowest possible mass flow through the control valve. The weak extinction limit for all injectors is at least $\Phi = 0.4$ or smaller, which is significantly better than for a kerosene injector of the same size and loading. The self-induced thermoacoustic response of all injectors is unremarkable. All measured temperatures, such as wall and heat shield, are well within the material limits. The test result figures contain an added frame showing the seal and heat shield contour, to approximate the burner outlets, and to show indicating arrows in orange for the air flow and in green for the fuel passage. The arrows are angled if representing a radial component but not scaled by the mass flow or velocity. As described in Sect. 3.2, the window frame is visible in the water vapor contour plots, but the injector axis is for both cameras at R/D = 0. The injector outlet is approximated as a contour and the arrows indicate the presence or absence of a radial component in the air flow, in orange, or the fuel flow, in green. The colour bars in Fig. 8a apply to all result figures and are normalized by the found maximum signal over all test conditions, after each image is scaled by its exposure time.

Two distinct test points are shown. The lean test point is extracted during the startup sequence at a normalized injector AFR of 1.8 for V2 and 2.51 to 2.61 for all other injectors. These test conditions are all well within the lean regime and chosen to obtain as much of the reaction zone as possible within the limited field of view of the APZs windows. A comparable fuel rich test point at a normalized AFR of 1 is shown for all injectors but V3.

### 5.1 Injectors V1 and V2: fast mixing

Both injectors employ fuel injection in between two layers of air and both injectors feature an inner air swirler. These similarities are found in the resulting images: V1 is depicted in Fig. 8 and V2 in Fig. 9.

#### 5.1.1 Injector V1

Injector V1 is shown at an normalized injector lean AFR of 2.58 in Fig. 8b and an injector rich AFR of 1.0 in Fig. 8c . V1 features an inner and outer air swirler with the fuel injected axially in between both air flows. The OH*-signal in the lean case (Fig. 8b ) is found close to the injector outlet with a high intensity in an elongated shape marked *A*. The contours of water vapor radiation in black show a similarly elongated shape. The injector design suggests a central recirculation zone. The OH*-signal presence at the injector outlet between R/D = 0 and R/D = 0.5 can only be caused by the presence of hydrogen in this region. The low intensity and spread signal can be caused by an instationary movement of the combustion in this low velocity region. The higher impulse of the air stream renders it unlikely that the fuel penetrates the inner air axially, as the fuel is introduced, but that the fuel recirculates with the hot combustion products and reacts in the inner shear layer between recirculation and inner air. Despite it being unlikely that the fuel penetrates the inner air flow, the injection direction of hydrogen will support mixing with the inner air stream. This mixture is ignited and stabilizes in the region marked *A*. The air from the outer swirler at least partly passes the combustion zone in between inner seal contour and reaction zone marked by the black arrow.

The increased fuel mass flow shown in Fig. 8c relocates the OH*-signal peak *A* radially and axially. The inner recirculation of hot gas is visible in the water vapor signal. It is again assumed that the recirculated gas contains hydrogen which combusts in the inner shear layer in between R/D = 0 and 0.5 and stabilizes the flame, which is then followed by a combustion of inner air with fuel

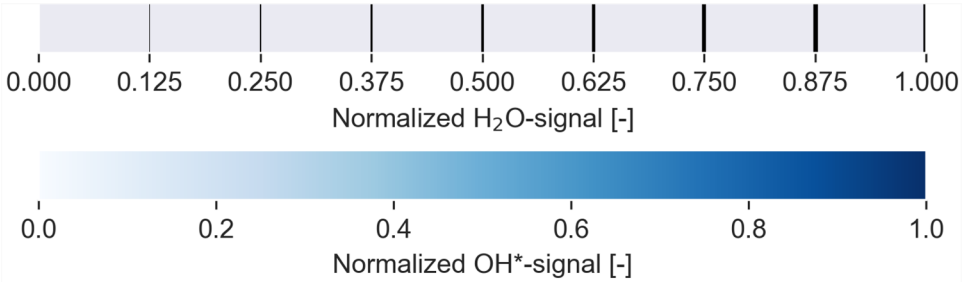


**(a)** Colour bar scaled to the common maximum of all images and applicable to all graphs within this publication

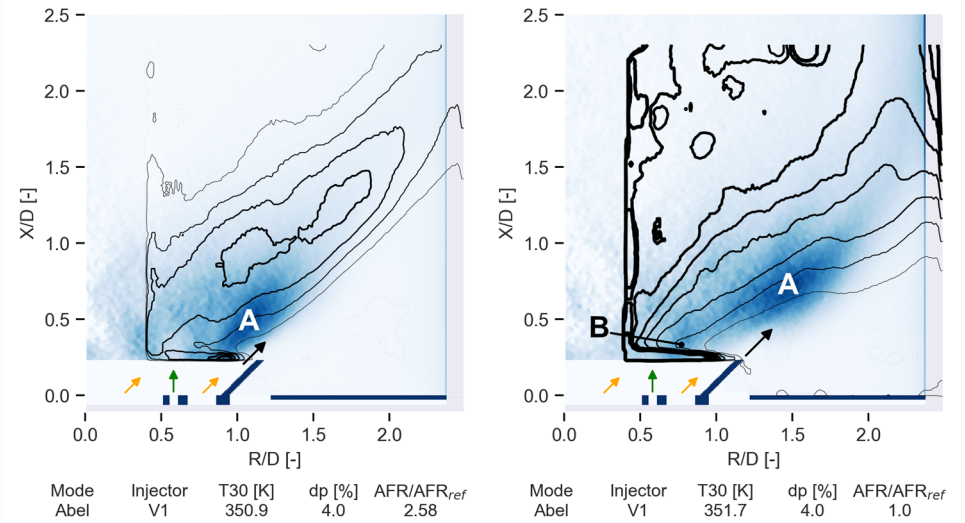


**(b)** V1 at a lean normalized AFR of 2.58 **(c)** V1 at a rich normalized AFR of 1.0

**Fig. 8** Colour bar and results of variant 1. In blue the OH*-signal overlaid with $H_2O$ vapor radiation contours

seen in the OH*-signal close to the seal outlet at the location marked *B*. Contrary to the lean case, the combustion region stretches over the continuation of the seal depicted by the black arrow. The water vapor radiation contours emerging from *A* curve towards the heat shield and fragments of hot combustion products can be seen on the heat shield and the outer seal lip. This indicates combustion with the cooling air in the shear layer of the outer recirculation.

### 5.1.2 Injectors V2

The design of V2 is similar to V1 in the location of the air and fuel flow paths, but it features a conical outlet for the swirled inner air, an angled fuel outlet without swirl as well as an unswirled angled outer air flow path. The injector lean test point (normalized AFR = 1.8) is shown in Fig. 9a and the injector rich test point (normalized AFR = 1) is displayed in Fig. 9b . The OH*-signal in the central region of the injector outlet is lower than in the case of V1, but still visible. An increased signal is found in the region marked *B*. The region with the highest intensity in OH*-signal is surrounding *A*. The injector appears to stabilise similarly to V1 through the recirculation of hot gas and hydrogen in the inner recirculation zone. The swirled inner jet, which at this point has a lower velocity due to the conical inner air flow path, mixes at the injector outlet with the fuel, and ignites due to the presence of recirculated gas from the inner recirculation zone. The flame propagates along the mixing region parallel to the seal contour in between inner air swirler and fuel towards *A*. This distinct streak in OH*-signal can be found also in Fig. 9b and c. Lastly, the combustion zone *A* forms with the outer air and in the outer recirculation entrained cooling air.

Reducing the AFR, thus increasing the fuel flow, at the same pressure drop leads to the averaged results shown in Fig. 9b . The centre of the injector shows a similar level of OH*-signal, but a strong signal of water vapor radiation. The central recirculation contains hot combustion products as well as recirculated hydrogen, which leads to OH*-signal in the region close to the centre of the injector outlet. Similarly, to the lean test case, the recirculated gas is causing the reaction of fuel with the inner

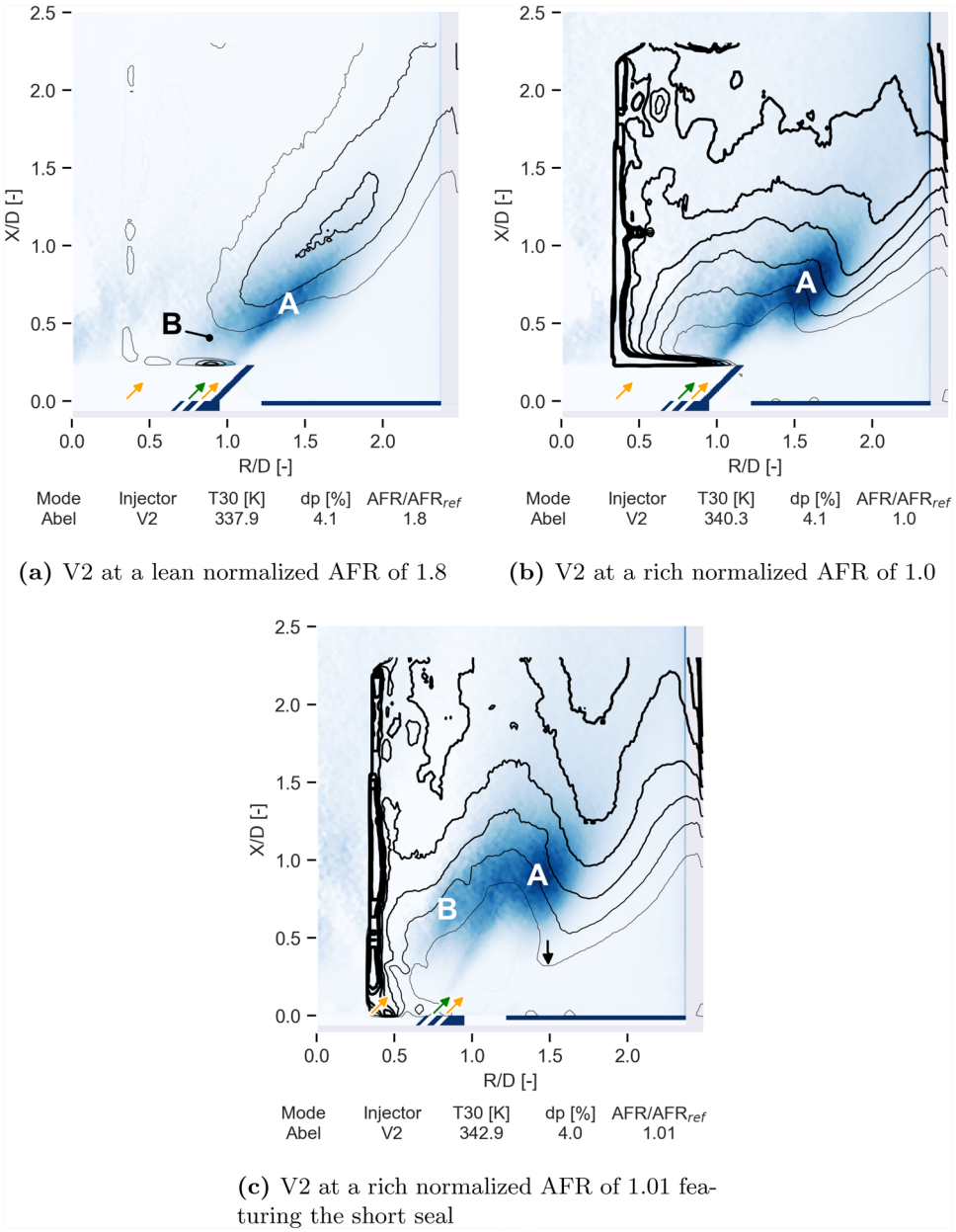


**Fig. 9** Results of variant 2 with the long and short seal. In blue the OH* signal overlaid with $H_2O$ vapor radiation contours

**(a)** V2 at a lean normalized AFR of 1.8

**(b)** V2 at a rich normalized AFR of 1.0

**(c)** V2 at a rich normalized AFR of 1.01 featuring the short seal

air swirler and leads to the characteristic fuel streak. The reaction zone *A* shows a higher maximum intensity and moves radially further outwards due to the larger quantity of fuel. Beside the zone being in the extension of the seal, the increased interaction with the outer recirculation and cooling air is shown in the water vapor contours curving towards the heat shield in the region *A*.

## 5.2 Injectors V3–V5: locally fuel rich

Similar to Sect. 5.1, the injectors V3, V4, and V5 are analysed in the following sections. All feature a central fuel injection surrounded by two air flows.

### 5.2.1 Injector V3

Variant 3 has a comparably large, central and not swirled fuel outlet. In the resulting image Fig. 10a of V3, the flame region is located in between the inner fuel flow and the two air swirlers. Both swirlers are co-rotating, with the inner air passage being smaller than the outer. A distinct differentiation between the two air flows based on the results cannot be found. The combustion region marked *A* starts close to the injector outlet and stretches all across the field of vision. An analysis of the stabilisation is not possible due to the seal limiting the visible space. The inner recirculation causes a second reaction on the inner side of the fuel flow (black arrow) above *B*. This flow regime is stable throughout the

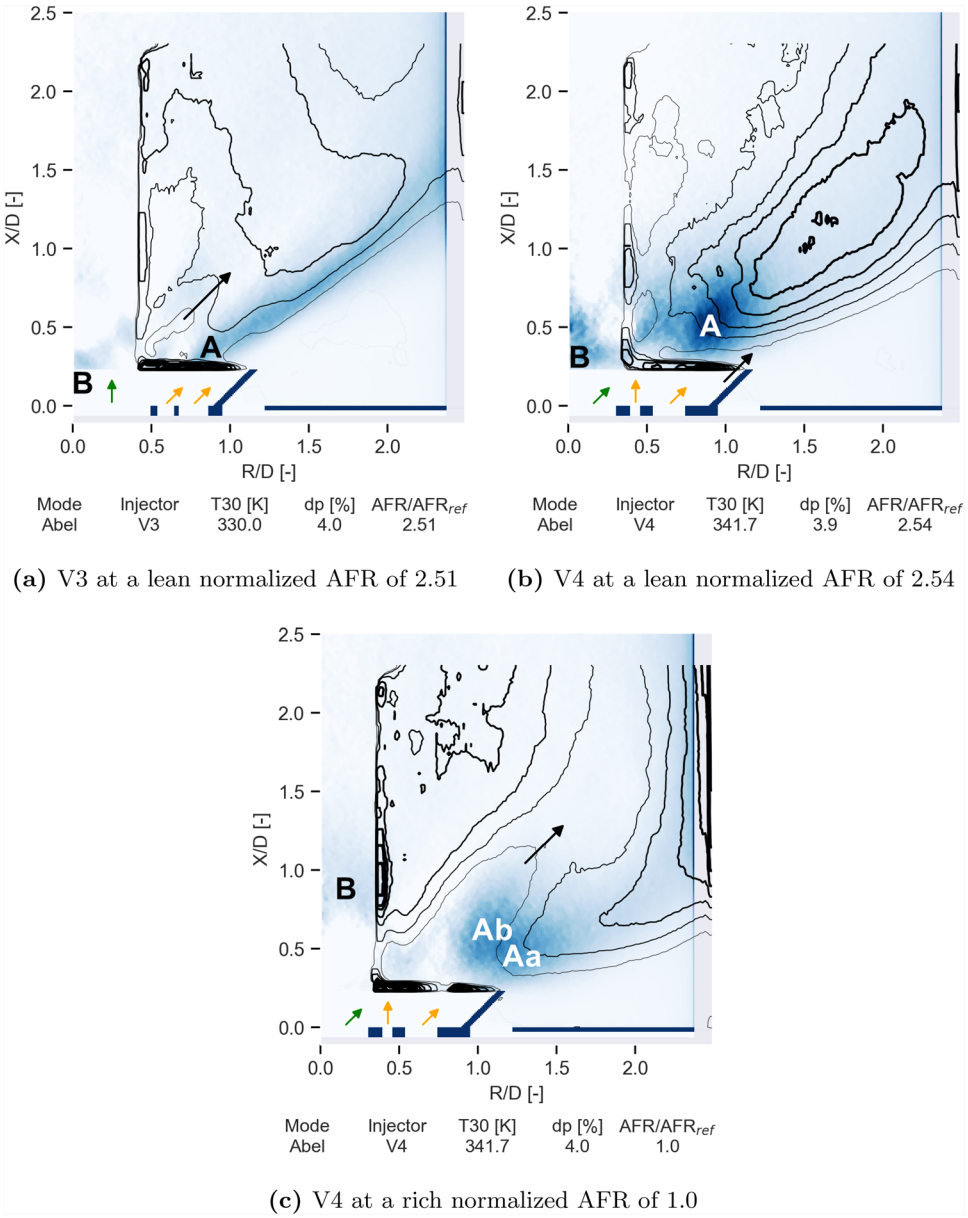


**Fig. 10** Results of variant 3 and variant 4. In blue the OH* signal overlaid with $H_2O$ vapor radiation contours

(a) V3 at a lean normalized AFR of 2.51

(b) V4 at a lean normalized AFR of 2.54

(c) V4 at a rich normalized AFR of 1.0

AFR variation and thus not shown at the rich condition. The inner combustion zone over *B* extends diagonally and the fuel flow wrinkling the water vapor contour line is more prominent with an increased fuel flow, but with a reduction in OH*-signal intensity close to the injector outlet where *A* is marked. The absence of entrained hot gas in the possible outer recirculation throughout all test points shows that fuel or hot products are not penetrating through the outer air flow.

### 5.2.2 Injector V4

V3 and V4 both feature a central fuel injection and two surrounding air flow paths. Contrary to V3, V4 is equipped with a fuel swirler and without an inner air swirler. An inner recirculation zone stretching into the fuel passage forms according to the CFD. The results shown in Fig. 10b replicate this recirculation in the OH*-signal: The inner recirculation transports oxidizer to the region marked *B*, where it combusts with the injected fuel. This stabilizing inner recirculation transports hot and reactive gas towards region *A*, where the fuel and the injector air partly mix and react. The part of the airflow that is not participating in the reaction zone *A* is marked with a black arrow. A hot zone of combustion products downstream of *A* can be seen in the water vapor contours as well as the inner recirculation.

The results of V4 at a fuel rich injector AFR are shown in Fig. 10c . The region *B* shifts downstream, which indicates that the increased fuel flow pushes the stagnation point of the inner recirculation downstream. The visible water vapor

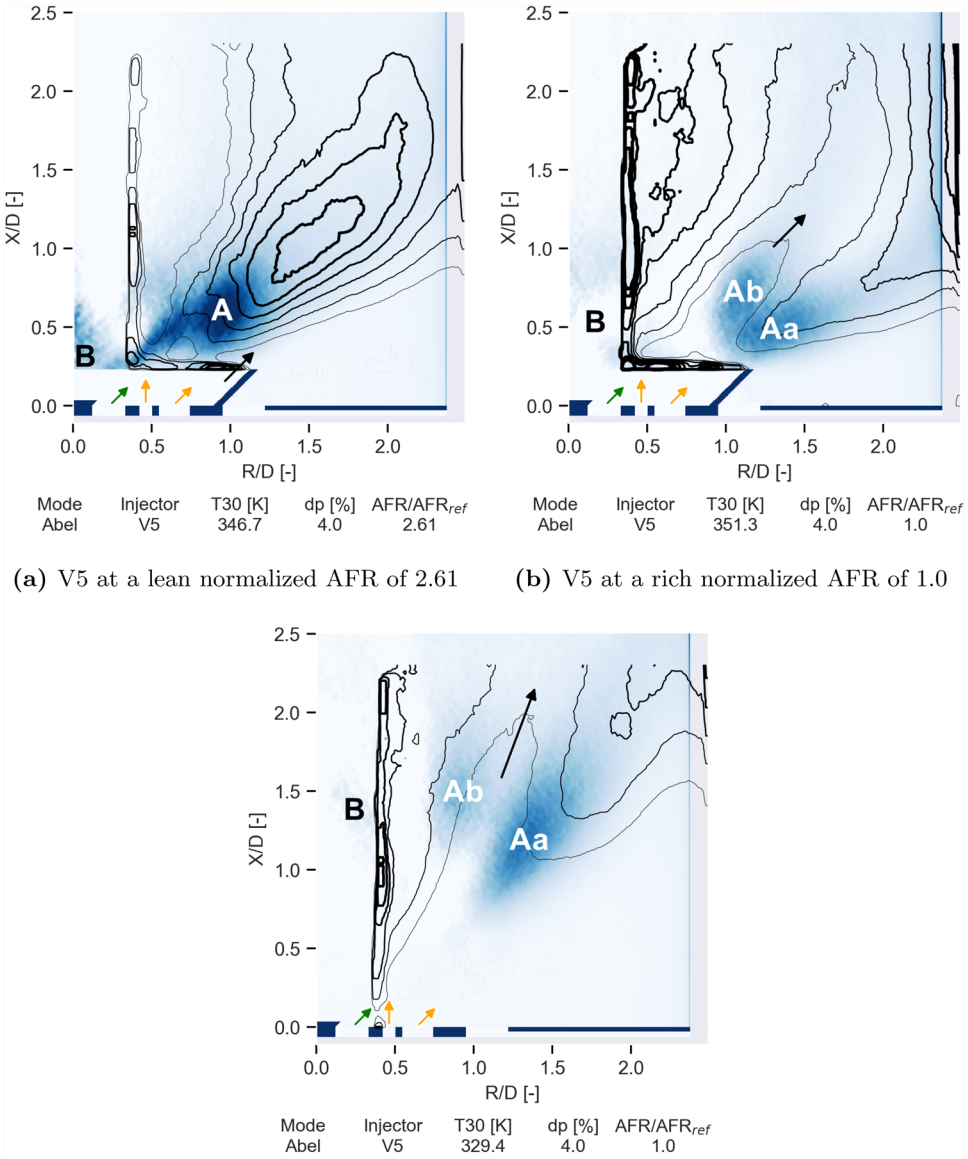


**(a)** V5 at a lean normalized AFR of 2.61

**(b)** V5 at a rich normalized AFR of 1.0

**(c)** V5 at a rich normalized AFR of 1.0 featuring the short seal

**Fig. 11** Results of V5 with long and short seal. In blue the OH* signal overlaid with $H_2O$ vapor radiation contours

contours closest to the central axis agree further downstream of the injector outlet (R/D = X/D ≈ 0.5). A faint OH*-signal imprint close to the outlet is found in between *B* and *Ab*. It is concluded, that the flame stabilizes as before due to the inner recirculation. The former reaction zone *A* is now spatially distributed into two regions *Aa* and *Ab*. The water vapor contour shows a colder streak around the black arrow. It is concluded that a part of the fuel penetrates both air flows and combusts fuel-rich in the region *Ab* with a part of the injector air and in *Aa* with injector air and additionally with cooling air. The comparatively colder streak marked by the black arrow is attributed to excess fuel.

### 5.2.3 Injector V5

V5 inherited all features of V4 and has an additional bluff body in the fuel stream. As expected, both show similar flow fields visible in Figs. 10a and 11b for the lean test point. The primary combustion zone *A* is similarly located. It can also be seen that the intensity for V5 is higher than for V4, which is correlated to the better penetration and mixing of fuel due to the higher fuel radial impulse by the bluff body and its guiding lip. The intense OH*-signal in *A* is attributed to the fuel mixing with the small inner air stream and also interacting with the shear layer of the outer air swirler. Again, as indicated by the black arrow, the fuel is not penetrating through the outer air flow. No interaction with the

corner recirculation is visible. The zone *A* is followed by a hot, elongated zone of combustion products. The OH*-signal at *B* leads to the conclusion that the flame stabilises in the shear layer of the central recirculation similarly to V4. According to the CFD, the bluff body creates a larger recirculation which ends at the sharp edge of the bluff body. The bluff body suppresses early interaction in between fuel and recirculated gas, thus the combustion is spatially more concentrated as shown by the prominent diagonal streak between *A* and *B* of OH* signal in the plot of V5 compared to V4.

Similarly, to the lean test point, also the rich test shown in Fig. 11b appears close to the results of V4 in Fig. 10c . Both regions *Aa* and *Ab* moved in positive R/D and X/D direction and separated, which leads to the assumption of a higher radial fuel outlet velocity. This can be caused by the deflecting lip on the bluff body and by the lightly lower effective area as shown earlier in Fig. 3. A higher interaction with the outer recirculation is expected due to the same reason. The inner combustion zone around *B* is pushed less downstream, which is ascribed to the wider opening of the fuel flow. Again, as in V4, a colder streak, which is expected to be excess fuel, can be found in the water vapor contours and is marked with a black arrow.

### 5.3 Influence of the short seal on V2 and V5

The longer seal employed in these tests is inherited from the kerosene injectors. The second seal, referred to as short or low seal, features no diverging section and does not protrude into the combustion chamber. According to the paragraph *The Nozzle Geometry* in chapter *5.5 Strong Swirl (S < 0.6)* in [28], the expected general functionality of the divergent seal is increasing the radial widening of the flow field and thus also, if applicable, the size of the central recirculation zone, if the flow field can follow the seal contour. V2 and V5 are tested with the short seal. The results are shown in Fig. 9c for V2 and Fig. 11c for V5. A central recirculation is assumed, since both show water vapor radiation on the combustor centre line. In both cases, the longer seal appears to previously have widened the flow field.

Comparing the OH*-signal of V2 in Fig. 9b and c shows how the combustion zone *A* moved axially upwards and radially inwards as expected. The signal of OH* and water vapor in the region below R/D = 0.5 and X/D = 1.0 both moved towards higher X/D, indicating that also the stagnation point of the recirculation moved in positive X/D direction. The diagonal streak of OH*-signal similar to V4 starting in the region of the fuel outlet prevailed, but with a lower intensity. Additionally, the inner recirculation shear layer stabilizes the flame in *B*, which is potentially overlapping with the diagonal streak in case of the longer seal and thus widened flow field. A larger outer recirculation is expected due to the narrower flow field. The combustion region *A* is stabilized interacting with this recirculation. The water vapor contours support the theory of a larger recirculation, since they spread further in negative X/D direction close to *A* and marked by the black arrow.

For V5, comparing Fig. 11b with Fig. 11c leads to the same assumption of a widening effect by the longer seal. The OH*-signals *Aa* and *Ab* separate and move in positive X/D direction and their elongated shapes turn counter clockwise. The assumption of stabilization in the shear layer of outer recirculation for the region *Aa* and inner recirculation for the region *Ab* is preserved. The black arrow in between indicates a similar colder streak of fuel containing gas. According to the assumption of a decreased inner recirculation, the centre line reaction *B* moved in positive X/D direction and the intensity and spatial distribution of visible water vapor radiation close to the injector centre line is reduced.

## 6 Conclusion

Five swirl stabilized hydrogen injectors for RQL combustion are tested in the APZ test bed. Recordings are taken in the UV spectrum to detect OH*-radicals and in the IR spectrum to capture water vapor radiation. The tests show that all injectors can be operated with hydrogen at all test points. Flame stabilization is observed in shear layers. The resistance against weak extinction reflects the wide combustion limits and high flame speeds of hydrogen. The diffusion injectors show no relevant level of self-induced thermoacoustic excitation. The wide range of injector designs tested was reproduced in the results. Fuel interacted with both air streams in variant 1 and 2 agreeing with the design objective of fast mixing. V3 shows a prevailing V-shaped combustion in between the central fuel injection and the air swirlers at all test points. The water vapor radiation contours of the fuel rich test cases of V4 and V5 show a colder and potentially fuel rich streak through the primary zone, which would agree with the design objective of achieving locally fuel rich regions.

The effect of the seal is shown for V2 and V5: In both cases the long and diverging seal widens the flow field and enhances recirculation. The reaction zones relocate accordingly and the water vapor contours show the altered recirculation zone.

Removing the seals divergent section reduces the thermal load on the seal, which was confirmed in the test campaign at the HBK-5 test bed [19]. Those tests were conducted using both long and short seals and the long seals showed concerning discoloration due to heat. Flame anchoring needs to be closely studied for future hydrogen injectors and

sharp edges similar to V4 and V5 can be of use to prevent anchoring.

A low-TRL-filter is established for application-oriented hydrogen jet engine combustion. Atmospheric conditions were used to scale down cost and experimental risk, which showed to be not deteriorating the performance of the low-TRL-filter. Based on initial CFD results, a wide range of injectors is early on manufactured and tested at low-risk conditions and with a streamlined measurement setup. Testing and design of the hydrogen injectors, accounting for the altered combustion characteristics of hydrogen, was adequately conducted despite lacking similar experience to kerosene equivalents. All injectors show promising characteristics and these results serve as initial data point for hydrogen jet engine injectors with operational capabilities. The goal of the study, to down-select promising concepts which also work in spatially and conditionally realistic combustion envelopes for the subsequent high-pressure tests, is achieved based on the successful test campaigns in the triple sector [17] and the full annular rig [19]. The presented results show high-potential for fast, low-cost and early stage experimental screening of hydrogen injectors.

The analysis of the flame stabilization in swirl stabilized hydrogen diffusion flames is conducted based on the OH*-signal and water vapor radiation. Beyond the extent of the presented low-TRL-filter, an experimental analysis of the flow field for a better analysis of the flame stabilization mechanism beyond the basic assessment of stability over the range of tested AFR is necessary to better interpret the findings. A well-tuned numerical simulation could further complement the findings and give insight into the local mixing and AFR distribution to design an injector based on the experimental results. Another assessment criterion of great interest are experimental $NO_x$ emissions, such as used in [17]. Assuming that V1 is closely related to a similar kerosene injector yields the conclusion that hydrogen flames stabilize faster than kerosene flames in the same flow field and at the same test point since the hydrogen flame, in case of the long seal, always partly burned within the seal.

The findings show that there is potential to further exploit the stability limits of hydrogen for RQL combustion. When applying a fast mixing concept, such as for V1 and V2, it might be beneficial to increase mixing more, but also reducing the AFR to achieve a stable, lifted flame. The primary zone size could then be reduced based on the desired combustion progress before entering the secondary zone. In a sense the concept behind V3, V4 and V5 already employed a spatially smaller, richer, and colder combustion zone within the original primary zone envelope. Further understanding the mixing and flame stabilization could yield a viable retrofit option from these injectors with reasonable $NO_x$ emissions.

**Acknowledgements** The authors acknowledge the funding from the German Federal Ministry for Economic Affairs and Climate Action (BMWK) in the framework of the LuFo project WOTAN under the grant agreement number (FKZ) 20M2104A (RRD) and 20M2104B (DLR). The authors would like to thank Ruud Eggels of RRD for his contribution regarding CFD-data and the management of RRD for their permission to publish this work. A special thanks is also reserved for the supporting engineers and mechanics who made testing possible.

**Author contributions** Carsten Clemen, Thomas Behrendt and Johannes Berger conceptualized the test campaign, whereas Carsten Clemen provided the injectors. The original draft was written by Johannes Berger and testing conducted by Johannes Berger and Sebastián Eisenring. The image processing was done by Johannes Berger and Sebastián Eisenring. Johannes Berger, Thomas Behrendt, Sebastián Eisenring and Carsten Clemen contributed to the discussion and interpretation. The campaign was supervised by Thomas Behrendt and Bertram Janus. All authors revised the manuscript.

**Funding** Open Access funding enabled and organized by Projekt DEAL. The research leading to these results has received funding from the German Federal Ministry for Economic Affairs and Climate Action (BMWK) in the framework of the LuFo project WOTAN under the grant agreement numbers (FKZ) 20M2104A (RRD) and 20M2104B (DLR). FKZ-20M2104B was used to finance changes to the test rig infrastructure related to the experiments, while FKZ-20M2104A was used for financing the experiments.

**Data availability** Please contact the corresponding author for data and materials upon reasonable requests.

## Declarations

**Conflict of interest** The authors have no relevant interests, both financial and non-financial, to disclose.



## References

1. Masson-Delmotte, V., Zhai, P., Pirani, A., Connors, S.L., Péan, C., Berger, S., Caud, N., Chen, Y., Goldfarb, L., Gomis, M.I., Huang, M., Leitzell, K., Lonnoy, E., Matthews, J.B.R., Maycock, T.K., Waterfield, T., Yelekçi, O., Yu, R., Zhou, B.: Climate Change 2021: The Physical Science Basis. Contribution of Working Group I to the Sixth Assessment Report of the Intergovernmental Panel on Climate Change. Cambridge University Press, Cambridge, United Kingdom and New York, NY, USA (2023). https://doi.org/10.1017/9781009157896

2. Brewer, G.D.: Hydrogen Aircraft Technology. Routledge, New York (1991). https://doi.org/10.1201/9780203751480
3. France, D.H.: Combustion characteristics of hydrogen. Int. J. Hydrogen Energy **5**(4), 369–374 (1980). https://doi.org/10.1016/0360-3199(80)90018-X
4. Rolls Royce plc: The Jet Engine. Wiley, Chichester (2015)
5. Staufer, M.: Combustion Chamber Assembly with Burner Seal and Nozzle as well as Guiding Flow Generating Equipment. US010808623B2. Patent (2020)
6. Behrendt, T., Frodermann, M., Hassa, C., Heinze, J., Lehmann, B., Stursberg, K.: Optical measurements of spray combustion in a single sector combustor from a practical fuel injector at higher pressures. In: *Proc RTO AVT Symposium on Gas Turbine Engine Combustion, Emissions and Alternative Fuels*, Lisbon, Portugal (1998)
7. Fischer, A., Lahiri, C., Clemen, C.: A direct comparison of flame-transfer matrices measurements between hydrogen and kerosene flames in the same combustor at realistic aero-engine conditions. Turbo Expo, vol. Volume 3B: Combustion, Fuels & Emissions, pp. 03–04032 (2025). https://doi.org/10.1115/GT2025-153683
8. Leroy, M., Mirat, C., Renaud, A., Vicquelin, R.: Stabilization of low-nox hydrogen flames on a dual-swirl coaxial injector. J. Eng. Gas Turbines Power (2023). https://doi.org/10.1115/1.4055711
9. Leroy, M., Mirat, C., Renaud, A., Puggelli, S., Vicquelin, R.: Investigation of dual-flame-front stabilization in partially premixed hydrogen flames using synchronized PIV/OH-PLIF. Turbo Expo, vol. Volume 3A: Combustion, Fuels & Emissions, pp. 03–04012 (2025). https://doi.org/10.1115/GT2025-151618
10. Leroy, M., Mirat, C., Renaud, A., Puggelli, S., Vicquelin, R.: A novel swirled tri-channel injector for hydrogen combustion. Turbo Expo, vol. Volume 3B: Combustion, Fuels & Emissions, pp. 03–04036 (2025). https://doi.org/10.1115/GT2025-153779
11. Eck, M.E.G., Nedden, P., Saldern, J.G.R., Orchini, A., Paschereit, C.O.: Characterization of a fluidically-variable swirl burner: effects of the imprinted swirl on flame shapes and emissions for hydrogen-methane blends. Turbo Expo, vol. Volume 3A: Combustion, Fuels & Emissions, pp. 03–04047 (2025). https://doi.org/10.1115/GT2025-152856
12. Premchand, C.P., Godse, S., Kolwyck, J., Alexander, L., Davenport, J., Acharya, R., Palies, P.: Fully premixed hydrogen-air swirl flames shapes and transient processes. Turbo Expo, vol. Volume 3A: Combustion, Fuels & Emissions, pp. 03–04037 (2025). https://doi.org/10.1115/GT2025-152560
13. Touzeau, Y., Petit, S., Irimiea, C., Blaisot, B., Pilla, G., Mohamed, A.K.: Experimental investigation of a non-premixed H2/air swirled flame at elevated pressure using optical diagnostics. Turbo Expo, vol. Volume 3A: Combustion, Fuels & Emissions, pp. 03–04009 (2025). https://doi.org/10.1115/GT2025-151547
14. Ballotti, A., Senatori, G., Galeotti, S., Andreini, A.: Design and numerical investigation of a swirl-stabilized hydrogen burner for aero engine applications. Turbo Expo, vol. Volume 3B: Combustion, Fuels & Emissions, pp. 03–04035 (2025). https://doi.org/10.1115/GT2025-153758
15. Liu, X., Zhang, Q.: Influence of initial pressure and temperature on flammability limits of hydrogen-air. Int. J. Hydrogen Energy **39**(12), 6774–6782 (2014). https://doi.org/10.1016/j.ijhydene.2014.02.001
16. Davis, D.W., Therkelsen, P.L., Littlejohn, D., Cheng, R.K.: Effects of hydrogen on the thermo-acoustics coupling mechanisms of low-swirl injector flames in a model gas turbine combustor. Proc. Combust. Inst. **34**(2), 3135–3143 (2013). https://doi.org/10.1016/j.proci.2012.05.050
17. Eisenring, S., Behrendt, T., Berger, J., Tiessen, P., Janus, B., Clemen, C.: High-pressure testing of hydrogen fuel injectors in a triple-sector rql-rig for the rolls-royce pearl 15 hydrogen demonstrator engine program. CEAS Aeronaut. J. (2025). https://doi.org/10.1007/s13272-025-00922-2
18. Clemen, C., Ravikanti, M., La Bianca, N., Eggels, R., Wurm, B., Young, K.: Considerations for hydrogen fueled aerospace gas turbine combustion sub-system design. In: *Turbo Expo: Power for Land, Sea, and Air*. https://doi.org/10.1115/GT2024-122593 . GT2024-122593
19. Clemen, C., Eggels, R., Gebel, G., Fischer, A., Wurm, B., Staufer, M., Ahrens, D., Lahiri, C.: Development of a Hydrogen Fuel Injector for the Rolls-Royce Pearl 15 Hydrogen Demonstrator Engine Program. DLRK2024-630008: Submitted to DLRK Congress 2024, Hamburg, Germany
20. Gövert, S., Berger, J., Lipkowicz, J.T., Soworka, T., Hassa, C., Behrendt, T., Janus, B.: Experimental and numerical investigation of hydrogen combustion in a dual-swirl burner for aero-engine applications. J. Eng. Gas Turbines Power (2024). https://doi.org/10.1115/1.4065925
21. Behrendt, T., Hassa, C., Mohamed, A., Faleni, J.-P.: In situ measurement and validation of gaseous species concentrations of a gas turbine model combustor by tunable diode laser absorption spectroscopy (tdlas). ASMEDC, Berlin, Germany (2008). https://doi.org/10.1115/GT2008-51258
22. Haber, L.C., Vandsburger, U., Saunders, W.R., Khanna, V.K.: An examination of the relationship between chemiluminescent light emissions and heat release rate under non-adiabatic conditions. In: *Turbo Expo: Power for Land, Sea, and Air*, vol. 78552, pp. 002–02041 (2000). American Society of Mechanical Engineers
23. Hardalupas, Y., Orain, M.: Local measurements of the time-dependent heat release rate and equivalence ratio using chemiluminescent emission from a flame. Combust. Flame **139**(3), 188–207 (2004). https://doi.org/10.1016/j.combustflame.2004.08.003
24. Zhao, M., Buttsworth, D., Choudhury, R.: Experimental and numerical study of oh* chemiluminescence in hydrogen diffusion flames. Combust. Flame **197**, 369–377 (2018). DOI: https://doi.org/10.1016/j.combustflame.2018.08.019
25. Koomen, J., Dammers, T., Demougeot, N., Stuttaford, P., Heinze, J., Stockhausen, G., Fleing, C.: High pressure testing with optical diagnostics of a hydrogen retrofit solution to eliminate carbon emissions. In: *Proceedings of ASME Turbo Expo 2022: Turbomachinery Technical Conference and Exposition (GT 2022). the American Society of Mechanical Engineers*, New York, N.Y. (2022). https://doi.org/10.1115/GT2022-82652
26. Rivière, P., Soufiani, A.: Updated band model parameters for h2o, co2, ch4 and co radiation at high temperature. Int. J. Heat Mass Transf. **55**(13–14), 3349–3358 (2012). https://doi.org/10.1016/j.ijheatmasstransfer.2012.03.019
27. Gibson, S., Hickstein, D.D., Yurchak, R., Ryazanov, M., Das, D., Shih, G.: PyAbel/PyAbel: v0.9.0. Zenodo (2022). https://doi.org/10.5281/ZENODO.7438595
28. Beér, J.M., Chigier, N.A.: Combustion Aerodynamics. Fuel and Energy Science Series. Applied Science Publisher Ltd, London (1972)
29. Keesee, C.L., Guo, B., Petersen, E.L.: Laminar flame speed measurements of kerosene-based fuels accounting for uncertainties in mixture average molecular weight. J. Eng. Gas Turbines Power (2021). https://doi.org/10.1115/1.4049886
30. Krejci, M.C., Mathieu, O., Vissotski, A.J., Ravi, S., Sikes, T.G., Petersen, E.L., Kérmonès, A., Metcalfe, W., Curran, H.J.: Laminar flame speed and ignition delay time data for the kinetic modeling of hydrogen and syngas fuel blends. J. Eng. Gas Turbines Power (2013). https://doi.org/10.1115/1.4007737
31. Hu, E., Huang, Z., He, J., Miao, H.: Experimental and numerical study on laminar burning velocities and flame instabilities of hydrogen-air mixtures at elevated pressures and temperatures.

Int. J. Hydrogen Energy **34**(20), 8741–8755 (2009). https://doi.org/10.1016/j.ijhydene.2009.08.044
32. Dimotakis, P.E.: Turbulent free shear layer mixing. In: *27th Aerospace Sciences Meeting* (1989). https://doi.org/10.2514/6.1989-262
33. Browand, F.K.: The structure of the turbulent mixing layer. Physica D **18**(1), 135–148 (1986). https://doi.org/10.1016/0167-2789(86)90168-5
34. El Helou, I., Skiba, A.W., Mastorakos, E.: Experimental investigation of soot production and oxidation in a lab-scale rich-quench-lean (rql) burner. Flow Turbul. Combust. **106**(4), 1019–1041 (2021)
35. Kruljevic, B., Darabiha, N., Durox, D., Vaysse, N., Renaud, A., Vicquelin, R., Fiorina, B.: Experimentation and simulation of a swirled burner featuring cross-flow hydrogen injection with a focus on the oh* chemiluminescence. Combust. Flame **273**, 113945 (2025) https://doi.org/10.1016/j.combustflame.2024.113945
36. Turns, S.R.: An Introduction to Combustion: Concepts and Applications, 2nd edn. McGraw-Hill series in mechanical engineering, McGraw-Hill, Boston, Mass (2000)